Light propagation and scattering in stratified media: a Green's tensor approach

Michael Paulus

Electromagnetic Fields and Microwave Electronics Laboratory, Swiss Federal Institute of Technology, ETH-Zentrum ETZ, CH-8092 Zurich, Switzerland, and IBM Research, Zurich Research Laboratory, CH-8803 Rüschlikon, Switzerland

Oliver J. F. Martin

Electromagnetic Fields and Microwave Electronics Laboratory, Swiss Federal Institute of Technology, ETH-Zentrum ETZ, CH-8092 Zurich, Switzerland

Received July 27, 2000; accepted October 26, 2000

We present a new technique for computing the electromagnetic field that propagates and is scattered in three-dimensional structures formed by bodies embedded in a stratified background. This fully vectorial technique is based on the Green's tensor associated with the stratified background. Its advantage lies in the fact that only the scatterers must be discretized, the stratified background being accounted for in the Green's tensor. Further, the boundary conditions at the different material interfaces as well as at the edges of the computation window are perfectly and automatically fulfilled. Several examples illustrate the utilization of the technique for the modeling of photonic circuits (integrated optical waveguides), the study of the optics of metal (surface plasmons), and the development of new optical lithography techniques. © 2001 Optical Society of America

OCIS codes: 220.3740, 230.0230, 240.0240, 240.6680, 290.0290, 310.0310.

1. INTRODUCTION

Vertical-cavity surface-emitting laser diodes with Bragg mirrors, complex lens systems with antireflecting coatings, optical amplifiers with multiple quantum wells, and structured masks for optical nanolithography are all examples of optical systems that rely on stratified media formed by stacks of material layers with different permittivities. Light propagation and scattering in stratified media therefore cover an extremely broad spectrum of applications.

When the system is a bare stratified structure formed only by different material layers stacked together, the propagation of light can be investigated by simple techniques such as the use of a transmission matrix.[1–4] However, most practical applications do not rely on a bare, stratified medium but rather also incorporate active elements in the stratified background: for example, a Bragg grating on the top of a multilayered waveguide, a metallic profile on a glass mask for optical lithography, a ridge at the surface of a semiconductor laser, and a trench to define a cavity in a semiconductor substrate.

The objective of this paper is to present a general technique for light propagation and scattering in such a system formed by a stratified background with embedded elements. The techniques available for the study of these systems depend on the particular geometry under study.[4–6] They include, for example, beam propagation methods,[7–10] discrete sources,[11,12] eigenmode expansions,[13–15] finite differences,[16] finite-difference time domain,[17–19] finite elements,[20,21] the method of lines,[22,23] ray tracing,[24,25] and transfer matrix.[26]

Our approach is related to the coupled dipole approximation (also known as the discrete dipole approximation). This powerful technique has been used extensively for scattering calculations in systems in an infinite homogeneous background.[27–30] It has also been applied to scatters on a surface, the simplest form of a stratified background.[31–33]

In the present paper we introduce a technique that can accommodate scatterers in a stratified background formed by an arbitrary number of layers. This method is described in Section 2. In Section 3 we discuss several application examples that illustrate the utilization of the technique in different domains of modern optics. We summarize our results in Section 4.

2. FORMALISM

A. Electric Field Integral Equation

The typical system that we want to study is depicted in Fig. 1. Several three-dimensional (3D) scatterers described by the permittivity $\varepsilon(\mathbf{r})$ are distributed in a 3D stratified background composed of L layers with different relative permittivities ε_i, $i = 1, \ldots, L$. Throughout the paper we consider nonmagnetic materials with relative permeability $\mu = 1$ and harmonic fields with time dependence $\exp(-i\omega t)$.

When this system is illuminated with an incident electric field $\mathbf{E}^0(\mathbf{r})$ propagating in the stratified background, the total field $\mathbf{E}(\mathbf{r})$ is given by the integral equation[30,34]

$$\mathbf{E}(\mathbf{r}) = \mathbf{E}^{(0)}(\mathbf{r}) + \int_V d\mathbf{r}' \mathbf{G}(\mathbf{r}, \mathbf{r}') \cdot k_0{}^2 \Delta\varepsilon(\mathbf{r}') \mathbf{E}(\mathbf{r}'), \quad (1)$$

where $\mathbf{G}(\mathbf{r}, \mathbf{r}')$ is the Green's tensor associated with the stratified background, k_0 is the wave number in vacuum, and $\Delta\varepsilon(\mathbf{r})$ is the dielectric contrast:

0740-3232/2001/040854-08$15.00

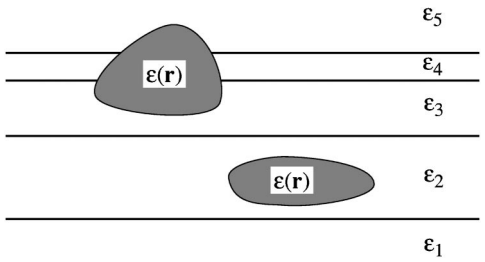

Fig. 1. Typical geometry under study: Several scatterers with permittivity $\varepsilon(\mathbf{r})$ are embedded in a stratified background composed of L layers with respective permittivity ε_i. Note that the first and last layers are semi-infinite media.

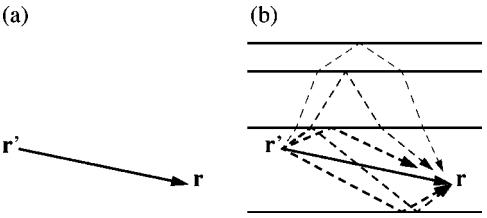

Fig. 2. The Green's tensor gives the electric field radiated at $\mathbf{r}$ by a dipole located at $\mathbf{r}'$, which (a) corresponds in an infinite homogeneous background to only direct radiation from $\mathbf{r}'$ to $\mathbf{r}$ and (b) further includes in a stratified medium all possible reflections at the $L-1$ interfaces.

$$\Delta\varepsilon(\mathbf{r}) = \varepsilon(\mathbf{r}) - \varepsilon_\kappa \quad \text{for } \mathbf{r} \in \text{layer } \kappa. \tag{2}$$

The integration in Eq. (1) runs on the volume of all the different scatterers $\varepsilon(\mathbf{r})$ in the structure.

It is important to note that the scatterers do not have to be embedded inside a background layer but can extend over several layers (Fig. 1). Further, these scatterers need not be homogeneous: $\varepsilon(\mathbf{r})$ can vary inside each scatterer. Finally, the permittivity of the scatterers does not necessarily have to be higher than that of their surroundings, and, for example, holes in a dielectric layer can be accounted for by use of a negative dielectric contrast $\Delta\varepsilon(\mathbf{r})$.

B. Green's Tensor for a Stratified Medium

The Green's tensor represents the response of a point source in the background. More precisely, each column β of the 3×3 matrix $G_{\alpha\beta}(\mathbf{r}, \mathbf{r}')$ gives the three components $\alpha = x,y,z$ of the electric field radiated at position $\mathbf{r}$ by a dipole located at position $\mathbf{r}'$ and oriented in the β direction ($\beta = x,y,z$).

For an infinite homogeneous background, this dyadic is just the field radiated directly from $\mathbf{r}'$ to $\mathbf{r}$ [Fig. 2(a)] and has a simple analytical form [see, e.g., Eq. (15) in Ref. 30].

Such is not the case for a stratified background. As illustrated in Fig. 2(b), the field radiated at $\mathbf{r}$ by a dipole located at $\mathbf{r}'$ now also includes the field reflected and refracted at all the interfaces. No analytical expressions exist in this case, and the Green's tensor must be computed numerically. This is quite a complicated task, which is best achieved by expressing the Green's tensor in reciprocal space (Fourier space) and using the symmetry properties of the background in that space. The Green's tensor is then obtained in direct space by means of inverse Fourier transform, i.e., by means of a numerical quadrature. This quadrature, which represents the core of the computation, is intricate because it involves several poles and branch cuts associated with the different electromagnetic modes that can be excited in the stratified background.

We recently developed an efficient computation technique for the evaluation of the Green's tensor in a stratified medium and refer the reader to Ref. 35, where the practical implementation of this technique is discussed in great detail. In the present paper we shall concentrate on the utilization of the Green's tensor for 3D scattering calculations in stratified media.

In that context, let us first discuss the evaluation of the integral in Eq. (1). For clarity, we use the following notation for the Green's tensor:

$$\mathbf{G}(\mathbf{r}, \mathbf{r}') = \begin{cases} \mathbf{G}^D(\mathbf{r}, \mathbf{r}') + \mathbf{G}^I(\mathbf{r}, \mathbf{r}') & \mathbf{r},\mathbf{r}' \text{ in same layer } \kappa \\ \mathbf{G}^I(\mathbf{r}, \mathbf{r}') & \mathbf{r},\mathbf{r}' \text{ in different layers} \end{cases}, \tag{3}$$

where $\mathbf{G}^D$ is the direct contribution and $\mathbf{G}^I$ accounts for the field reflected and refracted by all the interfaces [Fig. 2(b)]. Note that the direct tensor $\mathbf{G}^D$ is simply the Green's tensor associated with an infinite homogeneous polarizable background with permittivity ε_κ.[30]

When $\mathbf{r} \to \mathbf{r}'$, only the direct contribution $\mathbf{G}^D$ diverges because the direct interaction path vanishes while all the indirect interaction paths remain finite [the forthcoming discretization scheme will impose that the points where $\mathbf{G}(\mathbf{r}, \mathbf{r}')$ is computed are not on a boundary between two layers]. We can therefore handle the singularity of the Green's tensor in a similar manner as for an infinite homogeneous medium. Introducing Eq. (3) into Eq. (1) and taking the principal value as for Eq. (7) in Ref. 30, we obtain

$$\begin{aligned} \mathbf{E}(\mathbf{r}) = \mathbf{E}^0(\mathbf{r}) &+ \int_V d\mathbf{r}'\mathbf{G}^I(\mathbf{r}, \mathbf{r}') \cdot k_0^2\Delta\varepsilon(\mathbf{r}')\mathbf{E}(\mathbf{r}') \\ &+ \lim_{\delta V \to 0} \int_{V-\delta V} d\mathbf{r}'\mathbf{G}^D(\mathbf{r},\mathbf{r}') \cdot k_0^2\Delta\varepsilon(\mathbf{r}')\mathbf{E}(\mathbf{r}') \\ &- \mathbf{L} \cdot \frac{\Delta\varepsilon(\mathbf{r})}{\varepsilon_\kappa}\mathbf{E}(\mathbf{r}), \end{aligned} \tag{4}$$

where the infinitesimal volume δV centered at point $\mathbf{r}$ is used to exclude the singularity. The source dyadic $\mathbf{L}$, which depends on the shape of this exclusion volume δV, was derived in detail by Yaghjian.[36] Note in the last term of Eq. (4) the permittivity ε_κ of the layer where $\mathbf{r}$ is located. Note also that Eq. (4) is implicit for the unknown field $\mathbf{E}(\mathbf{r})$.

C. Discretized Equation

To solve Eq. (4) numerically, we define a mesh on the system with N discretized elements centered at $\mathbf{r}_i$ with permittivity $\varepsilon_i = \varepsilon(\mathbf{r}_i)$ and volume V_i. The only constraint for this discretization is that a given mesh must be entirely inside a layer and cannot sit astride a boundary between two layers (Fig. 3). The discretization volume V_i need not be constant. To achieve a given accuracy, it is

actually necessary to use a smaller mesh when the dielectric contrast is larger. To that extent, one can expect that the convergence of this scheme will be similar to that observed for scattering calculations in a homogeneous background. We refer the reader to Ref. 37, where this point was discussed in detail.

Keeping in mind that the discrete dielectric contrast $\Delta\varepsilon_i = \varepsilon_i - \varepsilon_\kappa$ depends on the permittivity of the layer κ where mesh i is located, we can write the discretized system of equations that correspond to Eq. (4):

$$\mathbf{E}_i = \mathbf{E}_i^0 + \sum_{j=1}^{N} \mathbf{G}_{i,j}^I \cdot k_0^2 \Delta\varepsilon_j \mathbf{E}_j V_j + \sum_{\substack{j \in \text{layer } \kappa \\ j \neq i}} \mathbf{G}_{i,j}^D \cdot k_0^2 \Delta\varepsilon_j \mathbf{E}_j V_j + \mathbf{M}_i \cdot k_0^2 \Delta\varepsilon_i \mathbf{E}_i - \mathbf{L} \cdot \frac{\Delta\varepsilon_i}{\varepsilon_\kappa} \mathbf{E}_i, \qquad i = 1, \ldots, N. \tag{5}$$

The self-term $\mathbf{M}_i$ is obtained in a similar manner as for an infinite homogeneous background:[30]

$$\mathbf{M}_i = \lim_{\delta V \to 0} \int_{V_i - \delta V} d\mathbf{r}' \mathbf{G}^D(\mathbf{r}_i, \mathbf{r}') = \frac{2}{3k_\kappa^2}[(1 - ik_\kappa R_i^{\text{eff}})\exp(ik_\kappa R_i^{\text{eff}}) - 1]\mathbf{1}, \tag{6}$$

where R_i^{eff} is the effective radius of mesh i:

$$R_i^{\text{eff}} = \left(\frac{3}{4\pi} V_i\right)^{1/3}. \tag{7}$$

For the integration in Eq. (6) we assumed a spherical exclusion volume δV. The corresponding source dyadic is[36]

$$\mathbf{L} = \frac{1}{3}\mathbf{1}. \tag{8}$$

Note in Eq. (6) the effective wave number $k_\kappa = k_0\sqrt{\varepsilon_\kappa}$ in layer κ.

The system of Eq. (5) represents the self-consistent interaction of N dipoles. Unlike for the coupled dipole approximation in vacuum, each dipole is now a dipole embedded in a stratified background, and the interaction includes all possible reflections and refractions at the $L - 1$ interfaces.

This system of equations is best solved numerically with an iterative solver.[29,38] Let us mention that, in a stratified medium, the Green's tensor does not have the same symmetry properties as in an infinite homogeneous background. In particular,

$$\mathbf{G}(\mathbf{r}, \mathbf{r}') \neq \mathbf{G}(\mathbf{r} - \mathbf{r}'). \tag{9}$$

It is therefore not possible to rewrite Eq. (1) as a convolution and to use a 3D fast Fourier transform to perform the integration.[39] It is, however, possible to use reduced symmetry properties in the x,y plane to expedite the computation.[33]

One of the advantages of the technique presented in this paper lies in the fact that only the scatterers must be discretized, the background being accounted for in the Green's tensor. Similarly, the interaction of scatterers located at large distances from one another does not require the discretization of the stratified background between them. Further, the complex boundary conditions at the edges of the computational window are automatically fulfilled, since they are included in the Green's tensor.

We mentioned that Eq. (1) is an *implicit* equation for the field $\mathbf{E}(\mathbf{r})$. Actually, this is the case only when $\mathbf{r}$ is located inside a scatterer. When $\mathbf{r}$ is located in the stratified background, Eq. (1) gives the field *explicitly* by integration on the scatterers' volume [$\Delta\varepsilon(\mathbf{r}') = 0$ when $\mathbf{r}'$ is in the background]. From a physical point of view, this means that knowledge of the field inside all the scatterers allows one to compute the field at any point in the stratified background. This can be used to expedite the calculation by first computing and storing the solution of Eq. (5) only for the discretized points inside the scatterers and then using this solution at a later stage to obtain the field in the background. Note that the last step does not necessitate the solution of a system of equations but requires only simple vector matrix multiplications.

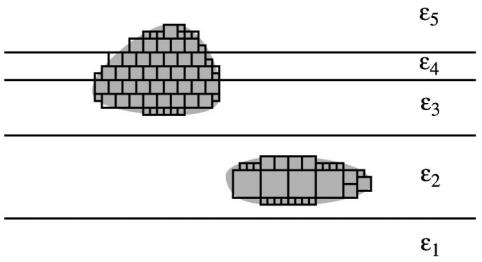

Fig. 3. Solving the scattering problem numerically requires that only the scatterers in the structure must be discretized. The sole constraint on the discretization is that a mesh cannot sit astride a boundary between two layers.

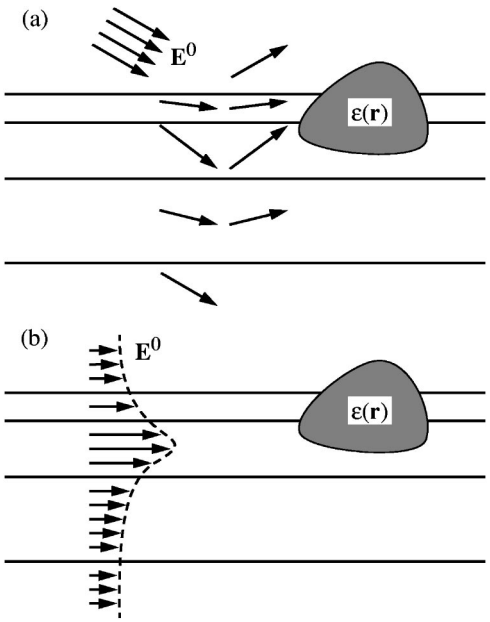

Fig. 4. The incident field must be a solution of the wave equation for the stratified background. It can correspond, for example, (a) to a plane wave impinging on the system or (b) to a waveguide mode propagating in the stratified background.

D. Incident Field

The incident field $\mathbf{E}^0(\mathbf{r})$ in Eq. (1) must be a solution of the wave equation in the stratified background. For a given geometry, this solution is not unique, as illustrated in Fig. 4. For example, the incident field can be a plane-wave excitation impinging on the stratified system [Fig. 4(a)]. In that case it must include all the multiple reflections inside the different layers. For the same geometry, $\mathbf{E}^0(\mathbf{r})$ could also be a waveguide mode propagating inside the structure [Fig. 4(b)] or even the field of a dipolar source embedded in the system. The latter can be used to investigate the radiation properties of a two-level molecule interacting with the system.[40]

3. APPLICATION EXAMPLES

In this section we present several examples that illustrate the application of our technique in domains as diverse as integrated optics, surface plasmons, and optical lithography.

A. Three-Dimensional Notch on a Planar Waveguide

As a first example, we consider a 3D notch of varying depth δ in a planar InP/InGaAsP waveguide (Fig. 5).[41] The notch has a finite extension (1 μm) in both the x and the y directions. For this geometry, only the air notch must be discretized, the associated polarizability $\Delta\varepsilon$ being negative, since the scatterer permittivity (air; $\varepsilon = 1$) is lower than the permittivity of the surrounding semiconductor. For the results presented in this section we use a $\Delta_x = \Delta_y = \Delta_z = 100$ nm discretization mesh.

At a wavelength $\lambda = 1.55$ μm, this waveguide supports a transverse electric mode (TE_0, electric field polarized in the y direction) and a transverse magnetic mode (TM_0, electric field polarized in the z direction).

We illustrate in Fig. 6 the electric field amplitude when this system is illuminated with a TE_0 mode propagating in the x direction (the mode is normalized so that the maximum electric field amplitude is unity). Some of the incident field is reflected by the notch, leading to an interference pattern caused by the interaction of the incident field with the reflected field. The incident mode is also scattered into the substrate and, to a lesser extent, into the air notch. These effects increase with the depth δ of the notch (note the different amplitude scales in Fig. 6). For the largest perturbation, the propagation of the mode in the forward direction is strongly disrupted [Fig. 6(c)].

In Fig. 7 we show the field amplitude distribution in the InGaAsP layer for the two mode excitations. Again the interference between incident and reflected fields is visible on the left-hand sides of the figures. The interaction of the incident field with the scatterer depends on the mode polarization. It is stronger for the TM_0 mode than for the TE_0 mode (note the different amplitude scales in Fig. 7). The disruption of the mode propagation in the forward direction, which leads to a dark shadow behind the notch, is clearly visible in Fig. 7. In spite of the finite lateral notch extension, it takes a large number of propagation wavelengths before the mode is reestablished in the waveguide (not shown).

Since our approach is fully vectorial and takes into account all the different field components, subtle effects such as polarization coupling can also be investigated.[42,43]

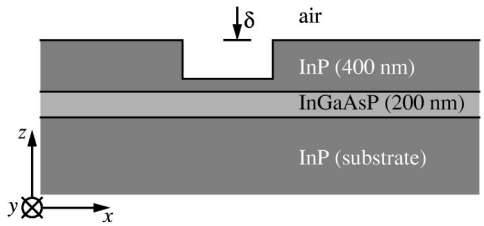

Fig. 5. A notch with a depth δ is etched in an InP/InGaAsP planar waveguide (permittivities $\varepsilon_{InP} = 10.05$ and $\varepsilon_{InGaAsP} = 11.42$; wavelength $\lambda = 1.55$ μm). The layer thicknesses are given in the figure. The notch has a finite extension (1 μm) in both the x and the y directions.

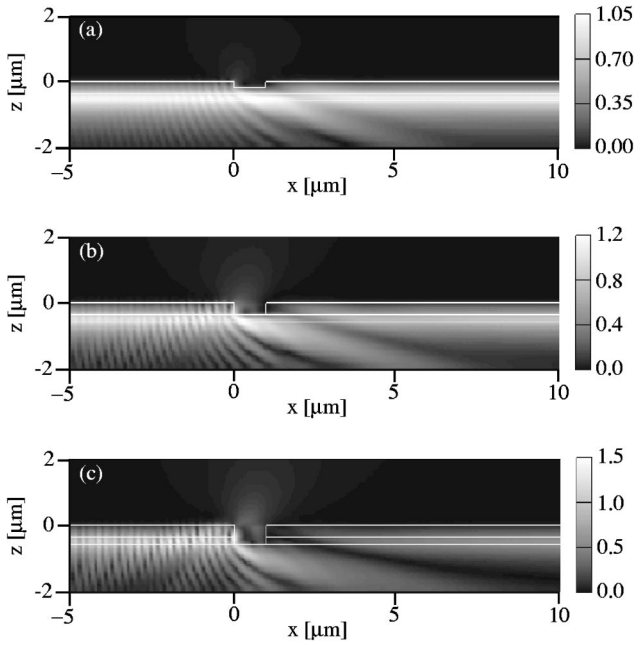

Fig. 6. Field amplitude at $y = 0$ in the structure depicted in Fig. 5 illuminated with a TE_0 mode propagating in the x direction. Three notch thicknesses are investigated: (a) $\delta = 200$ nm, (b) $\delta = 400$ nm, (c) $\delta = 600$ nm.

Figures 6 and 7 also illustrate how perfectly the boundary conditions at the edges of the computational window and at the different material interfaces in the stratified background are fulfilled. In particular, Fig. 6 shows the field scattered into the substrate and reflected backward to the incident direction; in Fig. 7 some of the field is scattered from the notch and escapes on the lateral sides of the computational window. In every case, the edges of the computational window remain perfectly transparent. This does not require any special treatment since these boundary conditions are already included in the Green's tensor.

B. Scattering of Surface Plasmons

Since our technique is not restricted to dielectric materials with a positive real part of the dielectric constant, we can also investigate the scattering of surface plasmons propagating along a metal–vacuum interface.[44]

In this example we excite a surface plasmon with the method of attenuated total reflection:[45] A *p*-polarized plane wave is incident on a planar glass–metal interface with an angle larger than the critical angle of total internal reflection (Fig. 8). Hence an exponentially decaying evanescent field is created in the metal layer. When the component of the wave vector parallel to the interface fulfills the eigenvalue equation for the surface mode, a plasmon is excited at the metal–vacuum interface (Fig. 8).

This plasmon propagates along the metal surface and interacts with any defect on it. As an example, we use the technique presented in Section 2 to investigate the scattering of such a plasmon with a dielectric protrusion

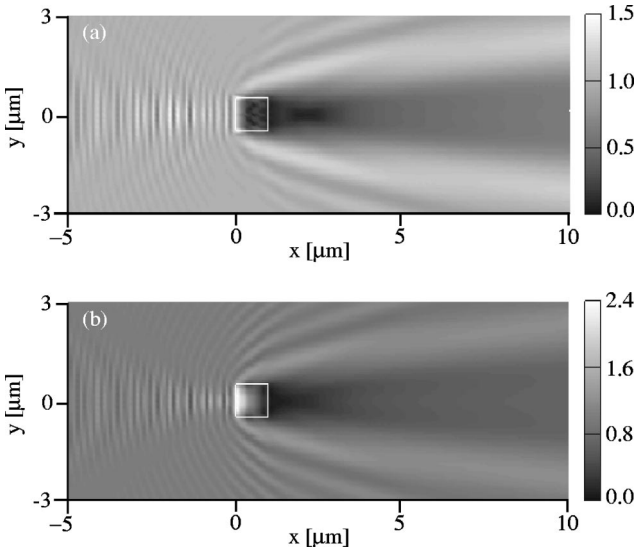

Fig. 7. Field amplitude in the InGaAsP layer ($z = -550$ nm) for the geometry depicted in Fig. 6(c) ($\delta = 600$-nm notch). The system is illuminated with two different modes, (a) TE_0 and (b) TM_0, propagating in the x direction. The maximum amplitude of each incident mode is normalized to unity.

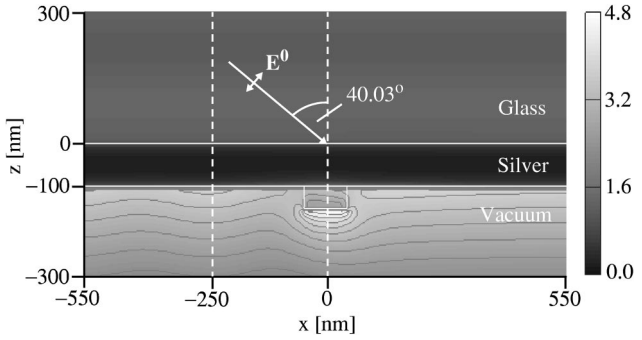

Fig. 8. Attenuated total reflection excitation of a surface plasmon. An incident field propagating in the glass substrate ($\varepsilon = 2.25$, $\lambda = 633$ nm) impinges at a 40.03° angle onto a 100-nm-thick silver film ($\varepsilon = -18.32 + i0.5$). This generates a surface plasmon propagating along the metal–vacuum interface. A $100 \times 100 \times 50$-nm^3 glass protrusion is deposited onto the silver surface. The electric field amplitude is shown. Note the scattering of the surface plasmon by the protrusion.

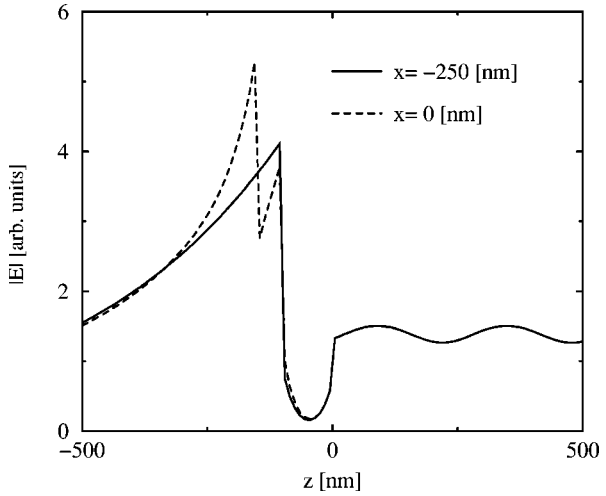

Fig. 9. Field amplitude along the two dashed lines in Fig. 8 ($y = 0$). Note the standing wave in the glass substrate and the localized plasmon field at the metal–vacuum, metal–glass, and glass–vacuum interfaces.

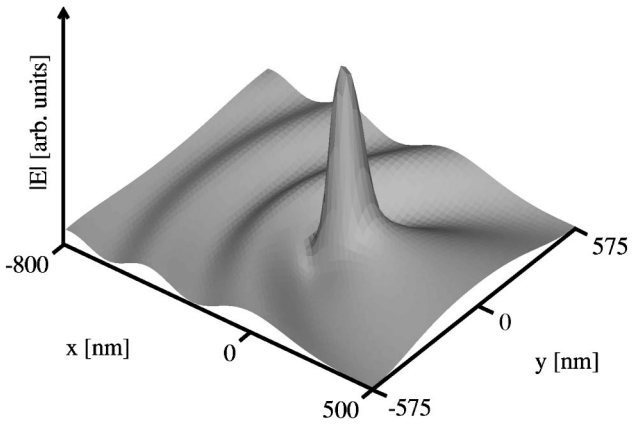

Fig. 10. Field amplitude in a constant-height plane in vacuum ($z = -155$ nm) below the glass protrusion (Fig. 8). Both the scattering and the confinement of the surface plasmon by the protrusion are visible.

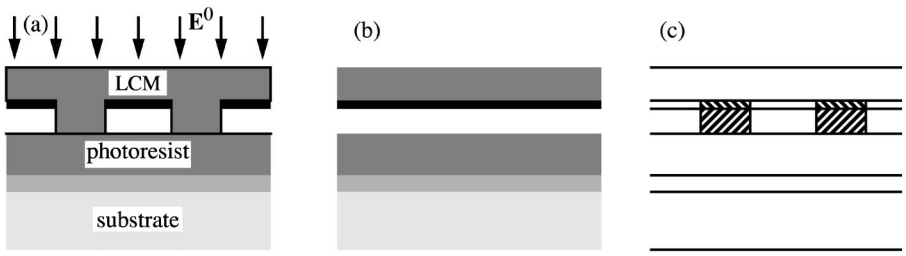

Fig. 11. LCM for optical nanolithography. (a) The structures to be written in the photoresist are defined as protrusions on a soft polymer substrate. This structure can easily be decomposed into (b) a stratified background with (c) embedded scatterers of various permittivities. A bottom antireflection coating (BARC) is deposited between the substrate and the photoresist.

deposited on the silver surface (the protrusion is discretized with $\Delta_x = \Delta_y = \Delta_z = 10\,\mathrm{nm}$).

The resulting field amplitude is illustrated in Fig. 8. A stationary wave is visible on the left side of the protrusion. It results from the interaction of the plasmon propagating in the positive x direction with the plasmon reflected by the protrusion.

In Fig. 8 the electric field appears to vanish inside the metal. Actually, the field amplitude profiles in Fig. 9 show that the electric field is strongly localized at the surface of the metal, which is characteristic of a plasmon. The stationary wave in the glass substrate resulting from the interaction of the incident field with the reflected field is also visible in this figure.

Notice in Fig. 9 that, because of the higher index, the field decays more rapidly in the glass than in vacuum.[45] The second peak that appears at the glass–vacuum interface is merely related to the continuity of the displacement field $\mathbf{D} = \varepsilon\mathbf{E}$. As a matter of fact, because the field associated with the plasmon is predominantly polarized in the z direction, i.e., normal to the glass–vacuum interface, it is the displacement field (not the electric field) that must be continuous.[46] The amplitude difference observed in Fig. 9 actually corresponds to the dielectric contrast between glass and vacuum. This depolarization effect has been discussed in detail in Ref. 47.

The strong field enhancement is evidenced in Fig. 10, where we show the field distribution in a plane parallel to the surface immediately below the protrusion. This figure clearly illustrates how the surface plasmon interacts with the glass protrusion.

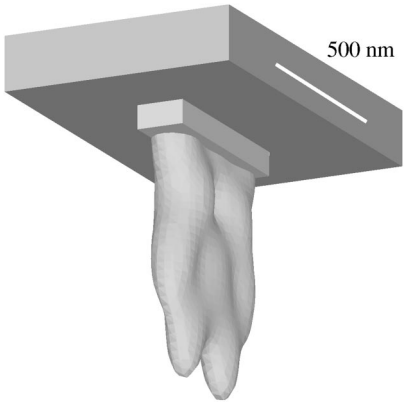

Fig. 12. LCM with a $120 \times 480 \times 75\,\mathrm{nm}^3$ protrusion. An isosurface of the field intensity distribution transmitted in the photoresist is shown. Such an isosurface corresponds to the profile of the structure that will be developed in the photoresist.

C. Optical Nanolithography

As last example, we consider a light-coupling mask (LCM) for optical lithography. This polymer mask has proved to be an efficient alternative for high-resolution lithography: Using 248-nm light, it allows one to define structures in the sub-100-nm range.[48,49]

The structures to be written in the photoresist are defined as protrusions on the mask, which will guide and focus the light into the photoresist (Fig. 11). To increase contrast, a thin gold layer is deposited inside the mask. The mask is illuminated from the top by circularly polarized light [Fig. 11(a)].

With our approach, only the protrusions must be discretized, as illustrated in Figs. 11(b) and 11(c). Note that, although the protrusions are made entirely of polymer, the discretized polarizability $\Delta\varepsilon_i$ that enters into the system of Eq. (5) is different for the meshes located in the gold absorber and those in the air layer [Fig. 11(c)]. For this example we use a $\Delta_x = \Delta_y = \Delta_z = 15\,\mathrm{nm}$ mesh.

Typical structures to be written on an integrated circuit are formed by so-called linelets with width d and length $4d$. Figure 12 shows an isosurface of the electric

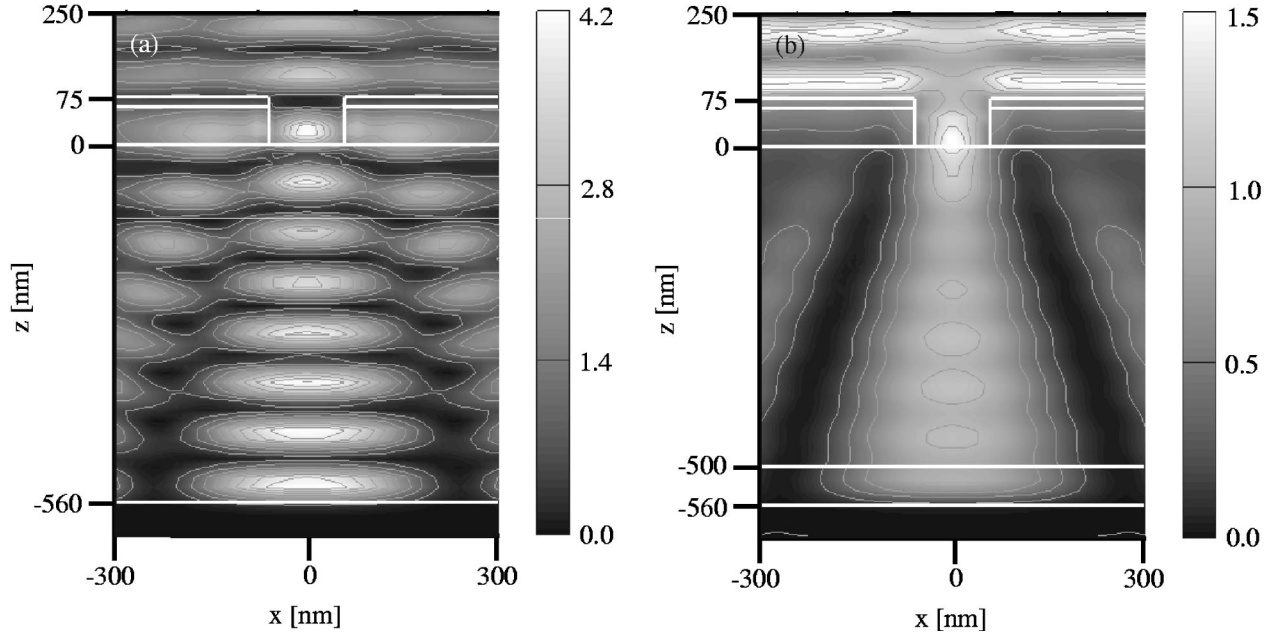

Fig. 13. (a) In a practical nanolithography experiment, reflections at the photoresist–substrate interface lead to a disturbing interference pattern in the photoresist. (b) To suppress this effect a 60-nm-thick BARC is deposited on the substrate. The electric field intensity is shown.

field intensity in the photoresist, below the LCM, for such an isolated linelet with $d = 120$ nm. This isosurface corresponds to the volume that will be exposed in the photoresist.[48] Such calculations are therefore useful for optimizing the exposition and assessing the ultimate resolution that can be achieved with this new lithography technique.

To avoid reflections at the resist–substrate interface, one usually includes an absorbing layer on top of the substrate before spinning the photoresist (Fig. 11).[50] The influence of such a 60-nm-thick bottom antireflection coating (BARC; $\varepsilon = 1.98 + i1.23$) is investigated in Fig. 13. Without the BARC we observe strong reflections from the substrate, leading to an interference pattern in the photoresist [Fig. 13(a)]. These disturbing interferences are suppressed by adding the BARC [Fig. 13(b)]. Note again in this figure how perfectly the boundary conditions are fulfilled at each medium interface as well as at the edges of the computation window.

4. CONCLUSION

It should be straightforward to implement in a computer the technique described in Section 2, together with the computation of the Green's tensor for a stratified medium detailed in Ref. 35.

The different examples presented in Section 3 illustrate the versatility of this new approach for propagation and scattering calculations in stratified media. This technique can be applied to a broad spectrum of problems ranging from classical optics to integrated optics and nanotechnology. Further, it can also be used to study the optics of metals.

ACKNOWLEDGMENTS

It is a pleasure to acknowledge stimulating discussions with A. Dereux, P. Gay-Balmaz, J. P. Kottmann, and C. Girard and to thank B. Michel and R. Vahldieck for their support of the project. We gratefully acknowledge funding from the Swiss National Science Foundation.

Address correspondence to Oliver J. F. Martin at martin@ifh.ee.ethz.ch.

REFERENCES

1. J. A. Kong, *Electromagnetic Wave Theory* (Wiley, New York, 1986).
2. M. Born and E. Wolf, *Principles of Optics*, 6th. ed. (Pergamon, Oxford, 1987).
3. L. B. Felsen and N. Marcuvitz, *Radiation and Scattering of Waves* (IEEE Press, Piscataway, N.J., 1994).
4. W. C. Chew, *Waves and Fields in Inhomogeneous Media* (IEEE Press, Piscataway, N.J., 1995).
5. R. März, *Integrated Optics Design and Modeling* (Artech House, Boston, Mass., 1994).
6. R. Scarmozzino, A. Gopinath, R. Pregla, and S. Helfert, "Numerical techniques for modeling guided-wave photonic devices," IEEE J. Sel. Top. Quantum Electron. **6**, 150–162 (2000).
7. W. P. Huang and C. L. Xu, "Simulation of three-dimensional optical waveguides by a full-vector beam propagation method," IEEE J. Quantum Electron. **29**, 2639–2646 (1993).
8. G. R. Hadley, "Low-truncation-error finite difference equations for photonics simulation. I. Beam propagation," J. Lightwave Technol. **16**, 134–141 (1998).
9. Y. Hsueh, M. Yang, and H. Chang, "Three-dimensional noniterative full-vectorial beam propagation method based on the alternating direction implicit method," J. Lightwave Technol. **17**, 2389–2397 (1999).
10. H. El-Refaei, D. Yevick, and I. Betty, "Stable and noniterative bidirectional beam propagation method," IEEE Photonics Technol. Lett. **12**, 389–391 (2000).
11. Y. A. Eremin and V. I. Ivakhnenko, "Modeling of light scattering by non-spherical inhomogeneous particles," J. Quant. Spectrosc. Radiat. Transf. **60**, 475–482 (1998).
12. C. Hafner, *Post-Modern Electromagnetics: Using Intelligent Maxwell Solvers* (Wiley, Chichester, UK, 1999).
13. C. M. Herzinger, C. C. Lu, T. A. DeTemple, and W. C. Chew, "The semiconductor waveguide facet reflectivity problem," IEEE J. Quantum Electron. **29**, 2273–2281 (1993).
14. J. Willems, J. Haes, and R. Baets, "The bidirectional mode expansion method for two-dimensional waveguides: the TM case," Opt. Quantum Electron. **27**, 995–1007 (1995).
15. H. Derudder, D. De Zutter, and F. Olyslager, "Analysis of waveguide discontinuities using perfectly matched layers," Electron. Lett. **34**, 2138–2140 (1998).
16. G. R. Hadley, "Low-truncation-error finite difference equations for photonics simulation. II. Vertical-cavity surface-emitting lasers," J. Lightwave Technol. **16**, 142–151 (1998).
17. J.-F. Lee, R. Palandech, and R. Mittra, "Modeling three-dimensional discontinuities in waveguides using nonorthogonal FDTD algorithm," IEEE Trans. Microwave Theory Tech. **40**, 346–352 (1992).
18. P. R. Hayes, M. T. O'Keefe, P. R. Woodward, and A. Gopinath, "High-order-compact time-domain numerical simulation of optical waveguides," Opt. Quantum Electron. **31**, 813–826 (1999).
19. A. Taflove and S. C. Hagness, *Computational Electrodynamics: The Finite-Difference Time-Domain Method*, 2nd ed. (Artech House, Boston, Mass., 2000).
20. J. B. Davies, "Finite element analysis of waveguides and cavities—a review," IEEE Trans. Magn. **29**, 1578–1583 (1993).
21. M. J. Noble, J. A. Lott, and J. P. Loehr, "Quasi-exact optical analysis of oxide-apertured microcavity VCSEL's using vector finite elements," IEEE J. Quantum Electron. **34**, 2327–2339 (1998).
22. S. F. Helfert and R. Pregla, "Analysis of thin layers and discontinuities," Opt. Quantum Electron. **31**, 721–732 (1999).
23. W. Huang and R. R. A. Syms, "Analysis of folded erbium-doped planar waveguide amplifiers by the method of lines," J. Lightwave Technol. **17**, 2658–2664 (1999).
24. E. Hasman, N. Davidson, Y. Danziger, and A. A. Friesem, "Diffractive optics: design, realization, and applications," Fiber Integr. Opt. **16**, 1–25 (1997).
25. D. R. Beltrami, J. D. Love, and F. Ladouceur, "Multimode planar devices," Opt. Quantum Electron. **31**, 307–326 (1999).
26. J. B. Pendry and P. M. Bell, "Transfer matrix techniques for electromagnetic waves," in Photonic Band Gap Materials, Vol. 315 of NATO ASI Series, C. M. Soukoulis, ed. (Kluwer, Dordrecht, The Netherlands, 1996), pp. 203–228.
27. G. H. Goedecke and S. G. O'Brien, "Scattering by irregular inhomogeneous particles via the digitized Green's function algorithm," Appl. Opt. **27**, 2431–2438 (1988).
28. B. T. Draine and P. J. Flatau, "Discrete-dipole approximation for scattering calculations," J. Opt. Soc. Am. A **11**, 1491–1499 (1994).
29. P. J. Flatau, "Improvements in the discrete-dipole approximation method of computing scattering and absorption," Opt. Lett. **22**, 1205–1207 (1997).
30. O. J. F. Martin and N. B. Piller, "Electromagnetic scattering in polarizable backgrounds," Phys. Rev. E **58**, 3909–3915 (1998).
31. M. A. Taubenblatt and T. K. Tran, "Calculation of light scattering from particles and structures on a surface by the

coupled-dipole method," J. Opt. Soc. Am. A **10**, 912–919 (1993).
32. C. Girard, A. Dereux, O. J. F. Martin, and M. Devel, "Generation of optical standing waves around mesoscopic surface structures: scattering and light confinement," Phys. Rev. B **52**, 2889–2898 (1995).
33. R. Schmehl, B. M. Nebeker, and E. D. Hirleman, "Discrete-dipole approximation for scattering by features on surfaces by means of a two-dimensional fast Fourier transform technique," J. Opt. Soc. Am. A **14**, 3026–3036 (1997).
34. C.-T. Tai, *Dyadic Green Function in Electromagnetic Theory* (IEEE Press, Piscataway, N.J., 1994).
35. M. Paulus, P. Gay-Balmaz, and O. J. F. Martin, "Accurate and efficient computation of the Green's tensor for stratified media," Phys. Rev. E **62**, 5797–5807 (2000).
36. A. D. Yaghjian, "Electric dyadic Green's functions in the source region," Proc. IEEE **68**, 248–263 (1980).
37. N. B. Piller and O. J. F. Martin, "Increasing the performances of the coupled-dipole approximation: a spectral approach," IEEE Trans. Antennas Propag. **46**, 1126–1137 (1998).
38. B. M. Nebeker, G. W. Starr, and E. D. Hirleman, "Evaluation of iteration methods used when modeling scattering from features on surfaces using the discrete-dipole approximation," J. Quant. Spectrosc. Radiat. Transf. **60**, 493–500 (1998).
39. M. F. Cátedra, R. P. Torres, J. Basterrechea, and E. Gago, *The CG-FFT Method* (Artech House, Boston, Mass., 1995).
40. G. W. Ford and W. H. Weber, "Electromagnetic interactions of molecules with metal surfaces," Phys. Rep. **113**, 195–287 (1984).
41. J.-J. He, B. Lamontagne, A. Delâge, L. Erickson, M. Davies, and E. S. Koteles, "Monolithic integrated wavelength demultiplexer based on a waveguide rowland circle grating in InGaAs/InP," J. Lightwave Technol. **16**, 631–638 (1998).
42. O. J. F. Martin, A. Dereux, and C. Girard, "Iterative scheme for computing exactly the total field propagating in dielectric structures of arbitrary shape," J. Opt. Soc. Am. A **11**, 1073–1080 (1994).
43. M. Paulus and O. J. F. Martin, "A fully vectorial technique for scattering and propagation in three-dimensional stratified photonic structures," Opt. Quantum Electron. (to be published).
44. A. D. Boardman, ed., *Electromagnetic Surface Modes* (Wiley, New York, 1982).
45. K. Welford, "The method of attenuated total reflections," in *Surface Plasmon-Polaritons* (Institute of Physics, Bristol, UK, 1988).
46. J. D. Jackson, *Classical Electrodynamics*, 3rd ed. (Wiley, New York, 1999).
47. O. J. F. Martin, C. Girard, and A. Dereux, "Dielectric vs. topographic contrast in near-field microscopy," J. Opt. Soc. Am. A **13**, 1801–1808 (1996).
48. H. Schmid, H. Biebuyck, B. Michel, and O. J. F. Martin, "Light-coupling masks for lensless, sub-wavelength optical lithography," Appl. Phys. Lett. **72**, 2379–2381 (1998).
49. H. Schmid, H. Biebuyck, B. Michel, O. J. F. Martin, and N. B. Piller, "Light-coupling masks: an alternative, lensless approach to high-resolution optical contact lithography," J. Vac. Sci. Technol. B **16**, 3422–3425 (1998).
50. H. A. Macleod, *Thin-Film Optical Filters*, 2nd ed. (Adam Hilger, Bristol, UK, 1986).